BMC Plant Biology

RESEARCH

Open Access

Integrative analysis of transcriptome and metabolome provides insights into the mechanisms of leaf variegation in *Heliopsis helianthoides*

Helan Qin[1*†], Jia Guo[1†], Yingshan Jin[1], Zijing Li[1], Ju Chen[2], Zhengwei Bie[3], Chunyu Luo[4], Feitong Peng[1], Dongyan Yan[1], Qinggang Kong[2], Fang Liang[1], Hua Zhang[1], Xuefan Hu[1], Rongfeng Cui[1] and Xiuna Cui[2]

Abstract

Background In the field of ornamental horticulture, phenotypic mutations, particularly in leaf color, are of great interest due to their potential in developing new plant varieties. The introduction of variegated leaf traits in plants like *Heliopsis helianthoides*, a perennial herbaceous species with ecological adaptability, provides a rich resource for molecular breeding and research on pigment metabolism and photosynthesis. We aimed to explore the mechanism of leaf variegation of *Heliopsis helianthoides* (using HY2021F1-0915 variegated mutant named HY, and green-leaf control check named CK in 2020 April, May and June) by analyzing the transcriptome and metabolome.

Results Leaf color and physiological parameters were found to be significantly different between HY and CK types. Chlorophyll content of HY was lower than that of CK samples. Combined with the result of Weighted Gene Co-expression Network Analysis (WGCNA), 26 consistently downregulated differentially expressed genes (DEGs) were screened in HY compared to CK subtypes. Among the DEGs, 9 genes were verified to be downregulated in HY than CK by qRT-PCR. The reduction of chlorophyll content in HY might be due to the downregulation of FSD2. Low expression level of PFE2, annotated as ferritin-4, might also contribute to the interveinal chlorosis of HY. Based on metabolome data, differential metabolites (DEMs) between HY and CK samples were significantly enriched on ABC transporters in three months. By integrating DEGs and DEMs, they were enriched on carotenoids pathway. Downregulation of four carotenoid pigments might be one of the reasons for HY's light color.

Conclusion FSD2 and PFE2 (ferritin-4) were identified as key genes which likely contribute to the reduced chlorophyll content and interveinal chlorosis observed in HY. The differential metabolites were significantly enriched in ABC transporters. Carotenoid biosynthesis pathway was highlighted with decreased pigments in HY individuals. These findings not only enhance our understanding of leaf variegation mechanisms but also offer valuable insights for future plant breeding strategies aimed at preserving and enhancing variegated-leaf traits in ornamental plants.

Keywords *Heliopsis helianthoides*, Transcriptome, Metabolome, Leaf variegation, FSD2, Carotenoid, ABC transporters, Ferritin

†Helan Qin and Jia Guo contributed equally to this work.

*Correspondence:
Helan Qin
saitougao123@outlook.com
Full list of author information is available at the end of the article

Introduction

Phenotypic mutations, particularly leaf color variations, represent common occurrences in the higher plants [1]. In the field of ornamental plants, leaf color mutations are often applied as a significant means for breeding new varieties. The breeding and application of ornamental foliage plants have significantly enriched the color palette of landscaping, substantially reducing maintenance costs. These developments hold considerable promise for the construction of ecologically adaptive urban landscapes. *Heliopsis helianthoides* is a perennial herbaceous plant from Asteraceae. It exhibits robust growth and possesses strong resistance to high temperatures, drought, and adverse soil conditions, making it recognized as an ecologically valuable species for landscaping. In the early studies of leaf color variation, researchers categorized leaf color mutants based on a significant amount of phenotypic data into various types, such as orange-yellow, yellowish-green, and yellow-white types [2, 3]. In recent years, a variegated-leaf variety of *Heliopsis helianthoides* coded as HY2021F1-0915 ("HY" is short for huaye which means variegated-leaf in Chinese) has been successfully cultivated in China, which is a potential research material for leaf color.

Research on plant leaf color variation has progressed beyond the analysis of phenotypic and physiological-biochemical characteristics, as well as the exploration of external factors influencing leaf color changes [4]. High-throughput sequencing technology (HTS) has brought about a revolutionary change compared to traditional Sanger sequencing. HTS holds significant value in deciphering the genetic information of unknown species' genomes and gene expression regulation [5]. The molecular-level investigation of leaf color changes is essential for understanding the mechanisms underlying leaf color formation in plants. For instance, transcriptome analysis has aided in finding the reason for yellow leaf color phenotype of *Populus deltoides* Marsh [6] and anthocyanin biosynthesis-related genes were identified as crucial genes leading to the color difference between yellow-leaf and red-leaf *Acer palmatum* [7]. The utilization of metabolomics has also considerably facilitated the discovery of active metabolites and their linked metabolic pathways in diverse plant species [8]. Metabolomics analysis has revealed the mechanism of leaf color change at three different stages of *Populus*×*euramericana* [9]. By integration of transcriptome and metabolome analysis, nine genes were identified as crucial genes in leaf coloration of *Fraxinus angustifolia* [10]. As an ornamental foliage plant, *Heliopsis helianthoides* might serve as valuable resources for molecular breeding and enhanced research into photosynthesis and the exploration of optimal materials for harnessing solar energy. The HY type cultivated in China has recently been observed to extend its ornamental period and to expand its potential for utilization as an excellent resource for investigating pigment metabolism, chloroplast development, differentiation, photosynthesis, and various related pathways. Unfortunately, there is a significant knowledge gap regarding the transcriptome and metabolome of *Heliopsis helianthoides*. Further research is therefore needed to explore the mechanisms behind variegated-leaves formation and to fully exploit the plant's resources. This research can yield valuable insights that contribute to the enhancement of the process of selecting and breeding plant varieties to maintain leaf variegation.

Materials and methods

Plant materials

The materials used in this study were self-bred varieties derived from the Beijing Institute of Landscape Architecture. The experimental group included variegated mutants named as HY derived from seedlings germinated after radiation treatment, characterized by white coloration between leaf veins. The variegated leaf traits remained relatively stable for three consecutive years through asexual reproduction. The control group consisted of plants (CK, short for control check) with normal green leaves.

In April 2019, the experimental materials were subjected to simultaneously cuttage in a greenhouse. Under the same environmental conditions (Night temperature/day temperature: 15℃-18℃/25℃-30℃; Relative humidity: 80% ± 5%) and management practices, they were potted in June, and transplanted in August with a plant spacing of 40×40 cm. Sampling and subsequent analyses were conducted in April, May, and June of 2020.

Sample collection and measurement of morphological traits and physiological parameters

Sample collection

Morphological assessments were conducted on sunny days from 10 to 12 AM in the early April to mid-June. Three HY individuals and three CK individuals were randomly chosen for each assessment. The second to third pairs of mature leaves below the apical bud were selected from each plant for measurement. For one of each pair of leaves, we measured the morphological traits and physiological parameters. The other leaf from each pair was picked for RNA and metabolite extraction.

Morphological traits measurement

The morphological traits measured in this study included the length, width, and thickness of the leaf under extension status. The measurement of each trait was repeated three times and the average was calculated. Leaf length

and leaf width were measured using a ruler, and leaf thickness was measured using a digital caliper. Leaf color was assessed indoors in accordance with the instructions of Royal Horticultural Society Colour Chart (RHSCC). In an indoor bright environment with natural light, the plant leaf was placed under the small hole of the color card that most closely matched its color, and the degree of color matching between the card color and the leaf color was observed within the hole. Finally the most matched color was confirmed. Leaf status of curling or extension was also recorded.

Physiological parameters measurement

Leaf Soil–Plant Analysis Development (SPAD) values, indicative of leaf color, were determined using a handheld SPAD-502 Chlorophyll Meter (Konica Minolta, Inc., Chiyoda City, Tokyo, Japan). Each leaf was measured three times at the fixed position near the leaf tip avoiding the midrib, and the average value was taken. Assimilation rate (A)(μmol·m^{-2}·s^{-1}), intercellular CO_2 concentration (Ci)(ppm), transpiration rate (E)(mmol·m^{-2}·s^{-1}), stomatal conductance (gs)(mmol·m^{-2}·s^{-1}), vapor pressure deficit (VPD) (mb), and water use efficiency (WUE) (CO_2 μmol·H_2O $mmol^{-1}$) were measured by CIRAS-3 Portable Photosynthesis System (PP Systems, Inc., Amesbury, MA, US). CIRAS-3 Portable Photosynthesis System was used on a sunny day, during the morning hours from 9:00 to 11:00. CIRAS-3's environmental parameters were checked, with CO_2 at 390 ppm, RH% at 100, and photosynthetically active radiation incident (PARi) at 1000 μmol·m^{-2}·s^{-1}. Healthy and consistent-age living leaves from the upper part of branches were selected for measurement.

Transcriptome sequencing

Total RNA was isolated using the Trizol reagent kit (Invitrogen, Carlsbad, CA, USA) following the manufacturer's instructions. RNA quality was evaluated using an Agilent 2100 Bioanalyzer (Agilent Technologies, Palo Alto, CA, USA) and verified through RNase-free agarose gel electrophoresis. Once the total RNA was obtained, mRNA was enriched using Oligo(dT) beads. Subsequently, the enriched mRNA was fragmented into shorter fragments using a fragmentation buffer and reverse-transcribed into cDNA using random primers. Second-strand cDNA was synthesized with DNA polymerase I, RNase H, dNTP, and buffer. Then the cDNA fragments were purified using the QiaQuick PCR extraction kit (Qiagen, Venlo, The Netherlands), subjected to end repair, had an A base added, and were then ligated to Illumina sequencing adapters. The ligation products were size-selected through agarose gel electrophoresis, PCR amplification, and subsequent sequencing on the Illumina Novaseq 6000 platform (Gene Denovo Biotechnology Co., Guangzhou, China).

The reads generated by the platform contained raw data that included adapters and low-quality bases, which could potentially interfere with subsequent assembly and analysis processes. Consequently, to obtain high-quality, clean reads, an additional filtering step was performed using the fastp software (version 0.18.0) [11] with the following standards: 1, Eliminating reads that contained adapters; 2, Discarding reads with more than 10% of unknown nucleotides (N); 3, Removing low-quality reads with more than 50% of bases having low quality (Q-value ≤ 20). De novo transcriptome assembly was conducted using the Trinity software [12], which is designed for the assembly of short reads.

The unigenes were annotated using the BLASTx program (http://www.ncbi.nlm.nih.gov/BLAST/) based on the following databases: the NCBI non-redundant protein (Nr) database (http://www.ncbi.nlm.nih.gov), the Swiss-Prot protein database (http://www.expasy.ch/sprot), the Kyoto Encyclopedia of Genes and Genomes (KEGG) database (http://www.genome.jp/kegg), and the COG/KOG database (http://www.ncbi.nlm.nih.gov/COG). Protein functional annotations were subsequently derived based on the top alignment results.

Weighted Gene Co-expression Network Analysis (WGCNA)

In this study, all statistical analyses were performed by R 4.2.0. Utilizing the "WGCNA" package [13], version 1.72.1], WGCNA was conducted based on gene expression values. The analysis commenced with the application of variance analysis to select the top 25% of genes for subsequent WGCNA analysis. Pearson correlation coefficients were then calculated for each pair of genes to select an appropriate soft threshold (β) that would ensure the constructed network adheres more closely to the characteristics of a scale-free network. Two common approaches were usually used to select the β-value: one was to choose the minimum power at which the correlation coefficients reach a plateau, and the other was to select a power where the correlation coefficients exceed the threshold of 0.8. Meanwhile, the mean connectivity of the network should also be taken into consideration when selecting β-value [14]. Next, A one-step approach was employed to build the gene network, whereby the adjacency matrix was transformed into a Topological Overlap Matrix (TOM). A hierarchical clustering tree of genes was also generated. Gene significance and module significance were calculated to measure the significance of genes in relation to physiological traits. This enabled theevaluation of the significance of gene-physiological trait associations. Additionally, significant associations

between modules and traits were analyzed to identify relevant gene modules.

Differential gene expression analysis

Using the "DESeq2" [15] in R, differentially expressed genes (DEGs) were selected based on the criteria of an absolute Log_2FC greater than 1 and an FDR < 0.05.

Functional enrichment analysis

Based on the results from WGCNA, gene modules were selected. For the genes within these modules, enrichment analyses including GO and KEGG enrichment analysis were performed using the "clusterProfiler" package [16], version 4.7.1.2]. Significantly enriched terms or pathways were screened through a filter criterion of p-value < 0.05.

Real-time quantitative reverse transcription PCR (qRT-PCR)

To further validate the expression of candidate genes, 13 DEGs related to leaf color were selected as candidate genes for qRT-PCR analysis. Total RNA was extracted from the leaves of CK plants and HY plants. After treatment with DNase I (amplification grade, Invitrogen, USA), cDNA was synthesized using oligo (dT) primers (Table 1) and SuperScript III Reverse Transcriptase kit (Thermo, USA). QRT-PCR experiments were conducted on ETC811 Thermal Cycler (Eastwin Scientific Equipments Inc., Suzhou, Jiangsu, China) with each gene analyzed in triplicate. Actin2 was used as an internal reference gene, and the formula for calculating the relative gene transcription levels was $2^{-\Delta\Delta ct}$ [17].

Chlorophyll content measurement

The fresh leaf samples were collected and chopped into small pieces. A 0.5 g sample was weighed and placed into a 10 mL capped centrifuge tube, which was then filled with 50℃ 80% acetone (Tianjin Fuyu Fine Chemical Co.,Ltd., Tianjin, China). After placing the tube in a dark environment for 48 h, the supernatant was directly analyzed. The determination of chlorophyll content was carried out using a UV-2700i UV–Vis spectrophotometer (Shimadzu Corporation, Kyoto, Japan) to measure the absorbance of the extract at wavelengths of 645 nm, 663 nm, and 652 nm. The content of chlorophyll a, chlorophyll b, and total chlorophyll can be calculated respectively according to the following formulas: chlorophyll a = $(12.7\ A_{665}\ -2.69\ A_{645}) \times \frac{V}{1000\times W}$; chlorophyll b = $(12.7\ A_{645}—2.69A_{665}) \times \frac{V}{1000\times W}$; total chlorophyll = $\frac{A_{652}}{34.5} \times \frac{V}{1000\times W}$.

Metabolomic analysis

The samples were ground using liquid nitrogen. A 25 mg portion of each sample was measured and placed into an EP tube, to which 500 µL of an extraction solution (methanol: water = 3:1, containing isotopically labeled internal standard mixture) was added. Subsequently, the samples underwent homogenization at 35 Hz for 4 min and were sonicated for 5 min in an ice-water bath. The ultrasound machine PS-60AL was procured from Shenzhen Leidebang Electronics Co., Ltd. (Shenzhen, China). This homogenization and sonication cycle was repeated three times. Following this, the samples were incubated for 1 h at -40℃ and then subjected to centrifugation at 12,000 rpm (RCF = 13,800(×g), R = 8.6 cm) for 15 min at 4℃. The supernatant was meticulously filtered through a 0.22 µm microporous membrane and transferred to a fresh glass vial for subsequent analysis. To create a quality control (QC) sample, an equal aliquot of the supernatants from all the samples was mixed.

Ultra-high-performance liquid chromatography-tandem mass spectrometry (UHPLC-MS/MS) analyses were conducted using a UHPLC system (Vanquish, Thermo Fisher Scientific, Waltham, MA, US) coupled with an Orbitrap Exploris 120 mass spectrometer (Orbitrap MS, Thermo) and a UPLC HSS T3 column (2.1 mm × 100 mm, 1.8 µm). The mobile phase consisted of 5 mmol/L ammonium acetate and 5 mmol/L acetic acid in water (A) and acetonitrile (B). The autosampler temperature was set at 4℃, and the injection volume was 2 µL. The Orbitrap Exploris 120 mass spectrometer was employed for its ability to acquire MS/MS spectra using information-dependent acquisition (IDA) mode within the control

Table 1 Primer sequences of qRT-PCR

Primer sequences	Primer	Products
FSD2 Forward primer	5′-CCGAGATTTCGGTTCGTTCG-3′	92bp
FSD2 Reverse primer	5′-CATACACAAGCCAAGCCCAA-3′	
STE1 Forward primer	5′-CCCACATGTAATCGCGTTGT-3′	133bp
STE1 Reverse primer	5′-TGCACCCATTACAGGCCATA-3′	
PIP1.4 Forward primer	5′-GAGGTTTCGAAGGCGGTAAC-3′	108bp
PIP1.4 Reverse primer	5′-ATGTGCCAACGATTTCAGCA-3′	
UXS2 Forward primer	5′-GAGCCGTTGTTGTTGGAAGT-3′	113bp
UXS2 Reverse primer	5′-AACGTCCCTACCACATTCGT-3′	
INPS1 Forward primer	5′-CTCTGTTGGCTGCTCCAATC-3′	117bp
INPS1 Reverse primer	5′-TTGTAGCCACCGGATGGAAT-3′	
MLP43 Forward primer	5′-CGCGGTGATGTCTTCCATAA-3′	97bp
MLP43 Reverse primer	5′-CACCTTCATGCAGCTCACAA-3′	
PGDH2 Forward primer	5′-GTTAACGCTCCCATGGTTCC-3′	131bp
PGDH2 Reverse primer	5′-ACCACCTTCACGGACTTGAT-3′	
PFE2 Forward primer	5′-ACGGTGATGTGCATTTAGCC-3′	156bp
PFE2 Reverse primer	5′-CACCTTCATGCAGGAGCATC-3′	
AGL65 Forward primer	5′-AGCCTGAAACATCGACAAGC-3′	140bp
AGL65 Reverse primer	5′-CATGGAAAGAGGGCATGAGC-3′	
18S Forward primer	5′-CGGCTACCACATCCAAGGAA-3′	191bp
18S Reverse primer	5′-GCTGGAATTACCGCGGCT-3′	

of the acquisition software (Xcalibur, Thermo). In this mode, the acquisition software continuously assessed the full scan MS spectrum. The electrospray ionization (ESI) source conditions were configured as follows: a sheath gas flow rate of 50 Arb, auxiliary gas flow rate of 15 Arb, capillary temperature of 320℃, full MS resolution set at 60,000, MS/MS resolution at 15,000, collision energy at 10/30/60 in normalized collision energy (NCE) mode, and spray voltage at 3.8 kV (positive) or -3.4 kV (negative), respectively.

The raw data were transformed into the mzXML format using ProteoWizard (https://proteowizard.sourceforge.io/) and subsequently subjected to processing using a program developed using R and reliant on the XCMS package for tasks including peak detection, extraction, alignment, and integration [18]. Subsequently, metabolite annotation was carried out utilizing an in-house MS2 database called BiotreeDB. The annotation threshold was set at 0.3.

Other statistical analysis

The significance of phenotype traits and physiological parameters differences between the CK and HY groups in April, May, and June were evaluated using a t-test, and a *p*-value of less than 0.05 was considered to indicate a significant difference.

Results

Morphological and physiological parameters of HY and CK individuals

This study has been based on different phenotypes of two *Heliopsis helianthoides* subtypes (Fig. 1A). Firstly, we recorded the morphological and physiological parameters of variegated-leaf HY individuals and green-leaf CK individuals in April, May and June to evaluate the leaves' differences. Visual comparisons between HY and CK leaf specimens revealed significant differences in leaf morphology. The CK leaves exhibited a classic, expansive form, whereas the HY leaves presented a subtle, yet distinctive curl (Fig. 1B). A quantitative analysis revealed that HY leaves were consistently shorter in length when juxtaposed with their CK counterparts throughout April to June. HY leaves were significantly narrower than those of the CK subtype, particularly in the months of May and June. The divergence in leaf thickness reached statistical significance solely in May, with HY leaves being relatively thinner. Employing the RHSCC color measurement system, we uncovered a striking difference in leaf pigmentation. The HY subtype exhibited a significantly higher RHSCC value across all three months, pointing to a more vibrant and lighter leaf coloration compared to the CK type (Fig. 1C).

The physiological data obtained from the HY and CK cohorts are depicted in Fig. 1C as well. The SPAD values, indicative of leaf color, were markedly diminished in the HY group relative to the CK group across the three-month period, suggesting the lighter leaf coloration in HY group, with a decline observed from April to June within the CK group. Notably, the intercellular CO_2 concentration exhibited a significant elevation in the HY group throughout April, May, and June. A trend was observed in the assimilation rate, which was initially higher in April for the HY group, yet experienced a decrease in May and June compared to the CK group. Additionally, the transpiration rate and stomatal conductance demonstrated a significant increase in the HY group as compared to the CK group in April. Furthermore, WUE revealed a significant reduction in the HY group throughout the three-month period.

Identification of SPAD-related genes co-expression modules by WGCNA

To identify genes related to leaf discoloration, we conducted WGCNA by integrating transcriptome data including 22,568 genes from samples collected in April, May and June with physiological parameter SPAD value. Initially, hierarchical clustering was performed on the expression levels of all genes in the leaf samples. Each sample was considered as a cluster, and the distances between these clusters were calculated. Ultimately, all samples were grouped into a single cluster, indicating the absence of outliers. Overall, the HY and CK samples were divided into different clusters (Fig. 2A). Subsequently, we identified a turning point where the mean connectivity curve began to level off. This turning point corresponded to a β-value of 7 and was also close to the 0.8 threshold (Fig. 2B). Using this threshold and the gene expression profiles, we conducted hierarchical clustering of modules (Fig. 2C). According to the merged dynamic results, all genes were categorized into 12 modules: greenyellow ($n=9382$); magenta4 ($n=2858$); mediumorchid ($n=2369$); orangered3 ($n=2099$); antiquewhite1 ($n=1486$); grey60 ($n=1416$); honeydew ($n=1247$); orangered4 ($n=645$); coral4 ($n=551$); mistyrose ($n=270$); darkseagreen2 ($n=178$); lightpink2 ($n=67$). Finally, we performed trait-related correlation analysis on these 12 modules.

The results revealed that the magenta4 and orangered3 modules exhibited the highest correlation with the SPAD trait, with correlation coefficients of -0.82 and 0.77, respectively (p-value < 0.05, Fig. 2D, Table S1). Significant correlation was found in gene significance and module membership, indicating that hub genes of magenta4 and orangered3 modules were correlated with SPAD (leaf color indicator) (Fig. 2E).

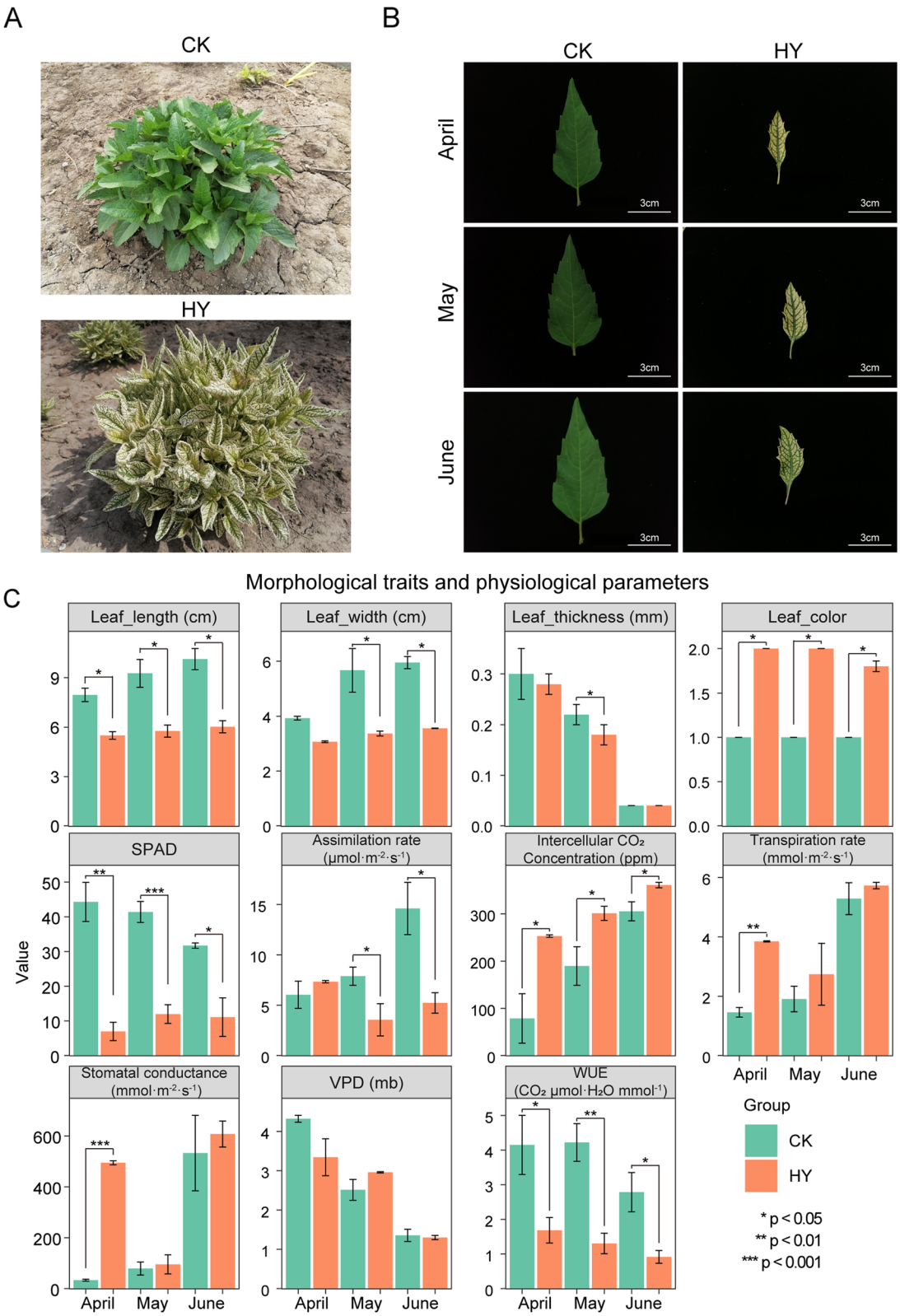

Fig. 1 Morphological and physiological parameters of CK and HY groups. **A** Representative photos of CK and HY subtypes. **B** Representative leaves of CK and HY individuals. **C** Morphological and physiological parameters of CK and HY subtypes

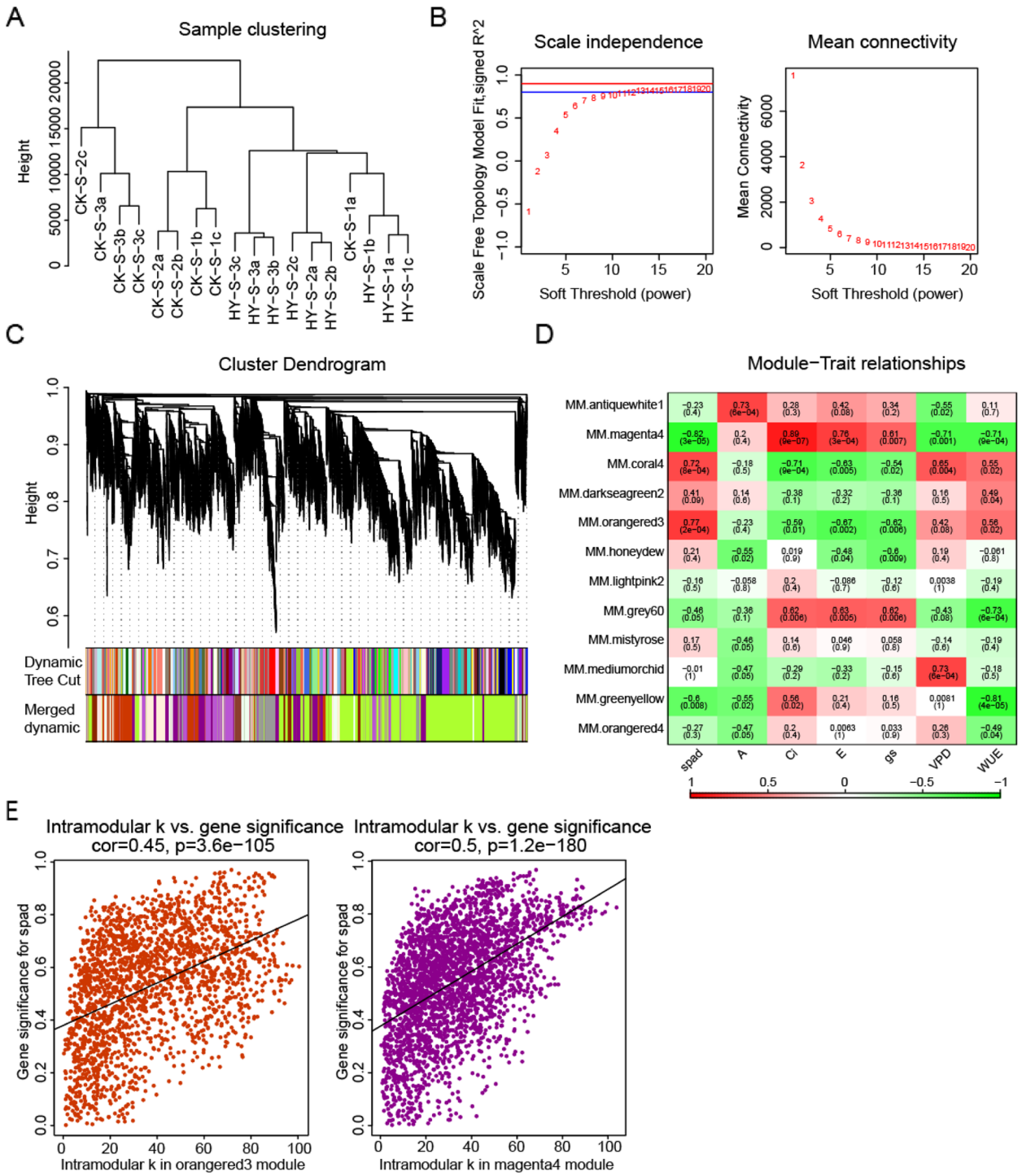

Fig. 2 Identification of SPAD-related genes co-expression modules by WGCNA. **A** Samples hierarchical clustering tree. "S" in the sample names means the upper part of plant, the numbers "1, 2, 3" represents April, May, and June respectively, and "a, b, c" indicates sample repeats. **B** Power value curve. In the left figure, the blue line indicated correlation coefficient of 0.8 and the red line indicated 0.9. **C** Gene dendrogram and module colors. **D** Heatmap of module-trait relationships. **E** Correlation between gene significance and module membership in magenta4 and orangered3 modules

Functional enrichment analysis of genes from SPAD-related modules selected via WGCNA

For the genes within the magenta4 and orangered3 modules, we conducted KEGG and GO functional enrichment analyses. In the magenta4 module, the genes were significantly enriched in 61 GO terms, such as "photosystem," "photosystem II," "photosynthetic membrane," "photosystem I reaction center," and "photosystem II reaction center" (Fig. 3A). Additionally, they were significantly enriched in 9 KEGG pathways, including "Photosynthesis" and "Photosynthesis—antenna proteins." (Fig. 3B). In the orangered3 module, genes were significantly enriched in 25 GO terms, including "magnesium chelatase complex" and "chloroplast" (Fig. 3C). Moreover, they were significantly enriched in 28 KEGG pathways, including "Metabolic pathways" and "Biosynthesis of secondary metabolites." (Fig. 3D). The detailed results can be found in Table S2.

Differential gene expression analysis between HY and CK individuals and their chlorophyll contents in different months

Besides screening leaf color-related genes by WGCNA, we also performed differential expression analysis between HY and CK samples from April to June to find candidate genes potentially influencing leaf color. Compared HY samples to CK samples, in April 5239 DEGs were identified (2714 upregulated, 2525 downregulated); in May, 6739 DEGs (3494 upregulated, 3245 downregulated) were identified; in June, 5594 DEGs (3133 upregulated, 2461 downregulated) were detected (Fig. 4A-C). Subsequently, DEGs at different time points were intersected with the genes in magenta4 and orangered3 modules determined by WGCNA, respectively, revealing there were 32 genes and 82 genes between the DEGs across all three time points and the magenta4, orangered3 module gene sets(Fig. 4D). Furthermore, we selected genes showing consistent differential expression trends between DEGs and WGCNA modules (magenta4, orangered3) across the three time points. A total of 9 genes in the magenta4_DEGs were consistently downregulated, and 17 genes in the orangered3_DEGs were consistently downregulated in HY individuals (Table S3). According to the results of qRT-PCR, 9 genes (FSD2, STE1, PIP1.4, UXS2, INPS1, MLP43, PGDH2, PFE2, AGL65) expressed significantly lower in HY group compared to CK group in all three months (Fig. 4E), with their expression levels from transcriptome in Figure S2. The downregulation of

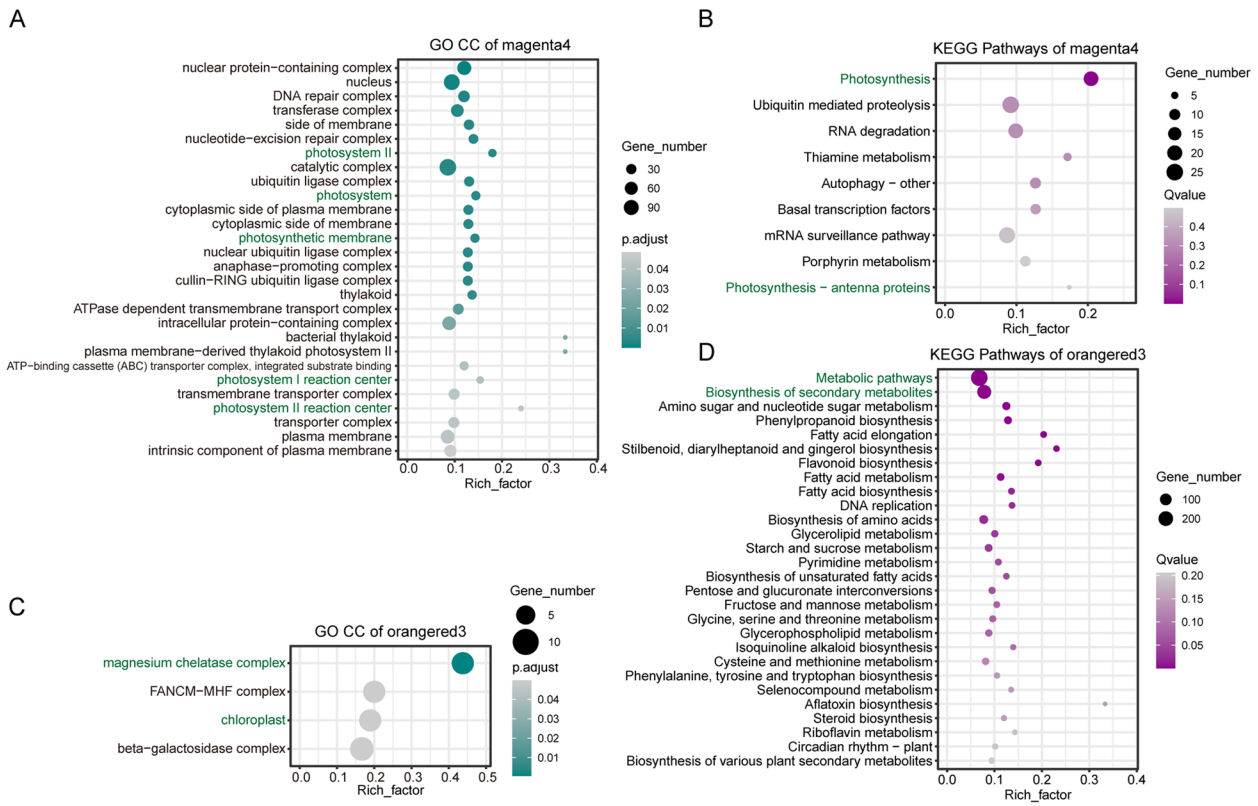

Fig. 3 Functional enrichment analysis of genes from SPAD-related modules selected via WGCNA. **A**, **B** GO and KEGG enrichment analysis of genes in magenta4 module. **C**, **D** GO and KEGG enrichment analysis of genes in orangered3 module

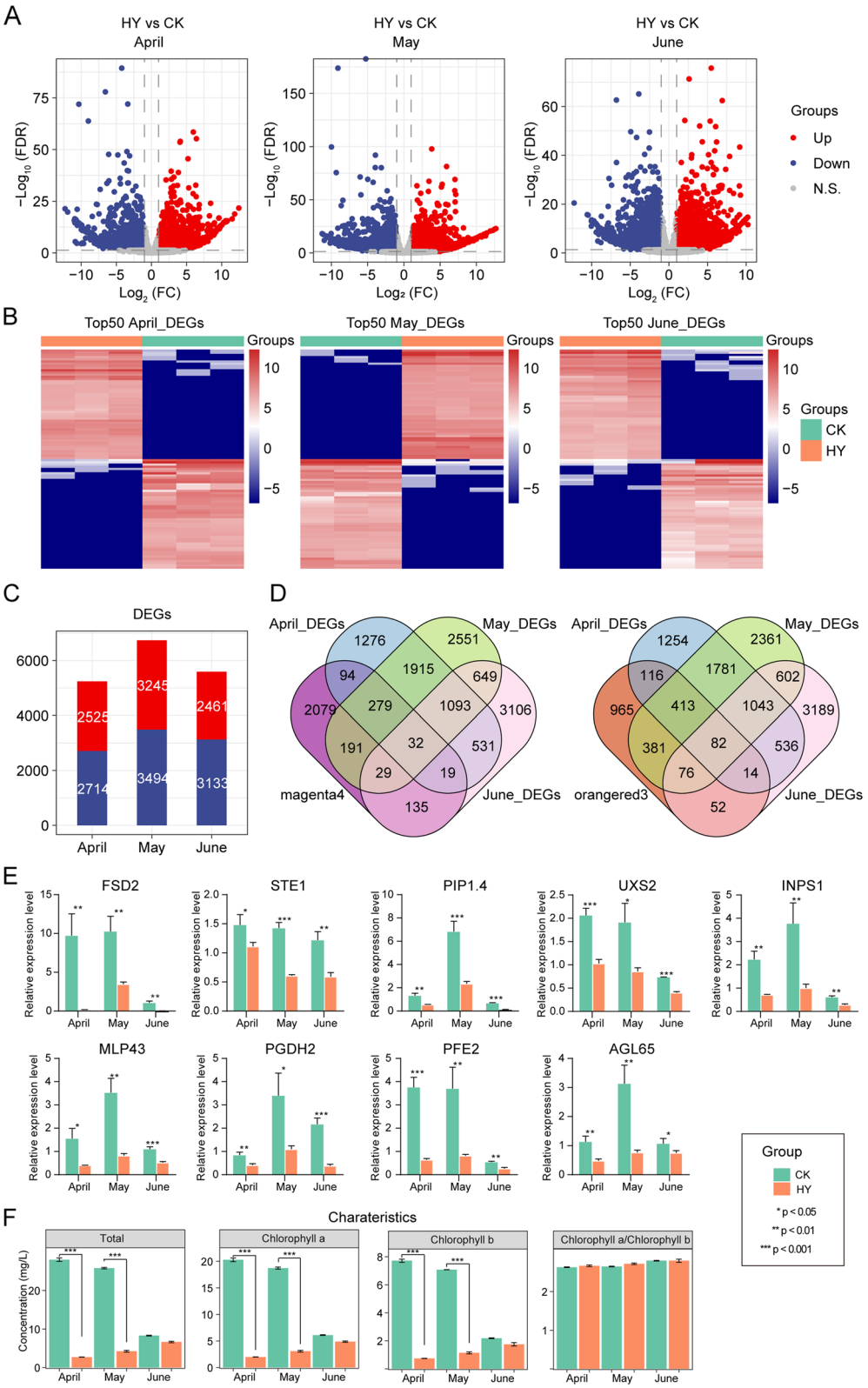

Fig. 4 Differential gene expression analysis between HY and CK individuals. **A** Volcano plot of DEGs between HY and CK leaves in April, May, and June. **B** Heatmap of top50 upregulated genes and top50 downregulated genes in HY compared to CK leaves in April, May, and June. **C** The number of DEGs in HY and CK individuals from April to June. **D** Intersection of DEGs and genes in magenta4 and orangered3 modules at different time points. **E** Results of qRT-PCR of 9 genes. **F** Chlorophyll contents of HY and CK from April, May, and June

genes such as FSD2 and PFE2, which were implicated in chlorophyll and iron homeostasis, respectively, might influence leaf color [19, 20].

Chlorophyll contents of HY and CK from April, May, and June were also monitored. In the CK group, a gradual decline was observed in the levels of total chlorophyll (28.01, 25.80, 8.30 mg/L), chlorophyll a (20.29, 18.72, 6.11 mg/L), and chlorophyll b (7.72, 7.08, 2.18 mg/L). In contrast, the HY group exhibited a notable increase in these chlorophyll metrics over the same period, with total chlorophyll contents reaching 2.72, 4.23, 6.64 mg/L, chlorophyll a contents reaching 1.98, 3.09, 4.89 mg/L, and chlorophyll b contents reaching 0.74, 1.14, 1.75 mg/L. Consistently across April, May, and June, the ratio of chlorophyll a to chlorophyll b maintained a balanced average of approximately 2.7 in both HY and CK plants, suggesting a stable photosynthetic apparatus. During April and May, the HY group displayed significantly reduced levels of total chlorophyll, chlorophyll a, and chlorophyll b in comparison to the CK group, a trend that correlated well with the SPAD values. However, by June, a shift occurredin the chlorophyll content in HY plants became statistically indistinguishable from that of CK (Fig. 4F). This divergence prompted the hypothesis that additional pigments might be influencing the leaf variegation pattern. Hence, we further detected the secondary metabolites.

Identification of SPAD-related metabolites modules by WGCNA

Besides transcriptome, metabolome was measured to dig secret of leaf variegation in *Heliopsis helianthoides*. A total of 1088 types of metabolites was detected in HY and CK samples. These metabolites were classified into 7 superclasses including alkaloids, amino acids and peptides, carbohydrates, fatty acids, polyketides, shikimates and phenylpropanoids, terpenoids.

To identify distinct metabolite modules highly correlated with the SPAD trait, serving as a quantitative measure of leaf color intensity, the same 18 samples as those used for transcriptome were used for WGCNA analysis, with no outliers present. The samples resulted in the segregation into three distinct categories corresponding to the months of April, May, and June. HY and CK samples were classified into separate branches within the clustering hierarchy (Fig. 5A). Next, a soft-thresholding power β of 16 was selected (Fig. 5B) to construct networks, yielding a total of 13 modules (Fig. 5C). The SPAD trait indicating leaf color was employed as the phenotype data for WGCNA. The correlation between each module and various traits was calculated (Fig. 5D). Modules with the highest absolute correlation to SPAD and a p-value less than 0.05 were selected, namely the greenyellow module (Fig. 5E) and the red module (Fig. 5F), which contained 42 and 93 metabolites, respectively (Table S4). Subsequently, to uncover the biological pathways that are significantly enriched and may be implicated in the regulation of leaf color, KEGG enrichment analysis was performed on these 135 metabolites, revealing enrichment in 9 pathways, where 2 of them were significantly enriched, namely tyrosine metabolism and vitamin B6 metabolism (Table S5, Fig. 5G).

Differential metabolomics analysis between HY and CK individuals

To investigate the variations in metabolite profiles between HY leaves and CK leaves at three different time points, we employed UHPLC-MS/MS to analyze the types of metabolites. Initially, principal component analysis (PCA) was employed to assess the degree of sample clustering and the overall distribution trends among the sample groups at the three time points. The results demonstrated clear separation between HY and CK groups at all three time points (Fig. 6A). Subsequently, the variable importance in projection (VIP) values for metabolites was computed using partial least squares discriminant analysis (PLS-DA), and metabolites with a p-value < 0.05 were selected as significantly different, names as differential metabolites (DEMs) (Fig. 6B). Top 10 upregulated and downregulated metabolites in April, May, and June were displayed in heatmaps (Fig. 6C). For samples in April, a total of 285 DEMs were identified in the HY compared to CK group, with 99 upregulated and 186 downregulated. In May groups, 235 DEMs were identified, comprising 65 upregulated and 170 downregulated in HY leaves. In samples collected in June, 324 DEMs were identified, including 104 upregulated and 220 downregulated in HY compared to CK group (Fig. 6D, Table S6). Next, the intersection of the DEMs at three time points was obtained, and 7 metabolites/35metabolites were shown to be upregulated/downregulated in HY from April to June (Fig. 6E). Furthermore, enrichment analysis was conducted separately for the DEMs between HY and CK groups at each time point. A total of 45, 28, and 44 KEGG pathways were significantly enriched in April, May and June respectively. (Fig. 6F, Table S7). In all three time points, pathways of ATP-binding cassette transporters (ABC transporters) and biosynthesis of cofactors were significantly enriched. Flavonoids are one of the major pigment categories in higher plants [21]. In May and June groups, the DEMs between HY and CK leaves were enriched on flavonoids and isoflavonoids syntheses potentially influencing leaf color.

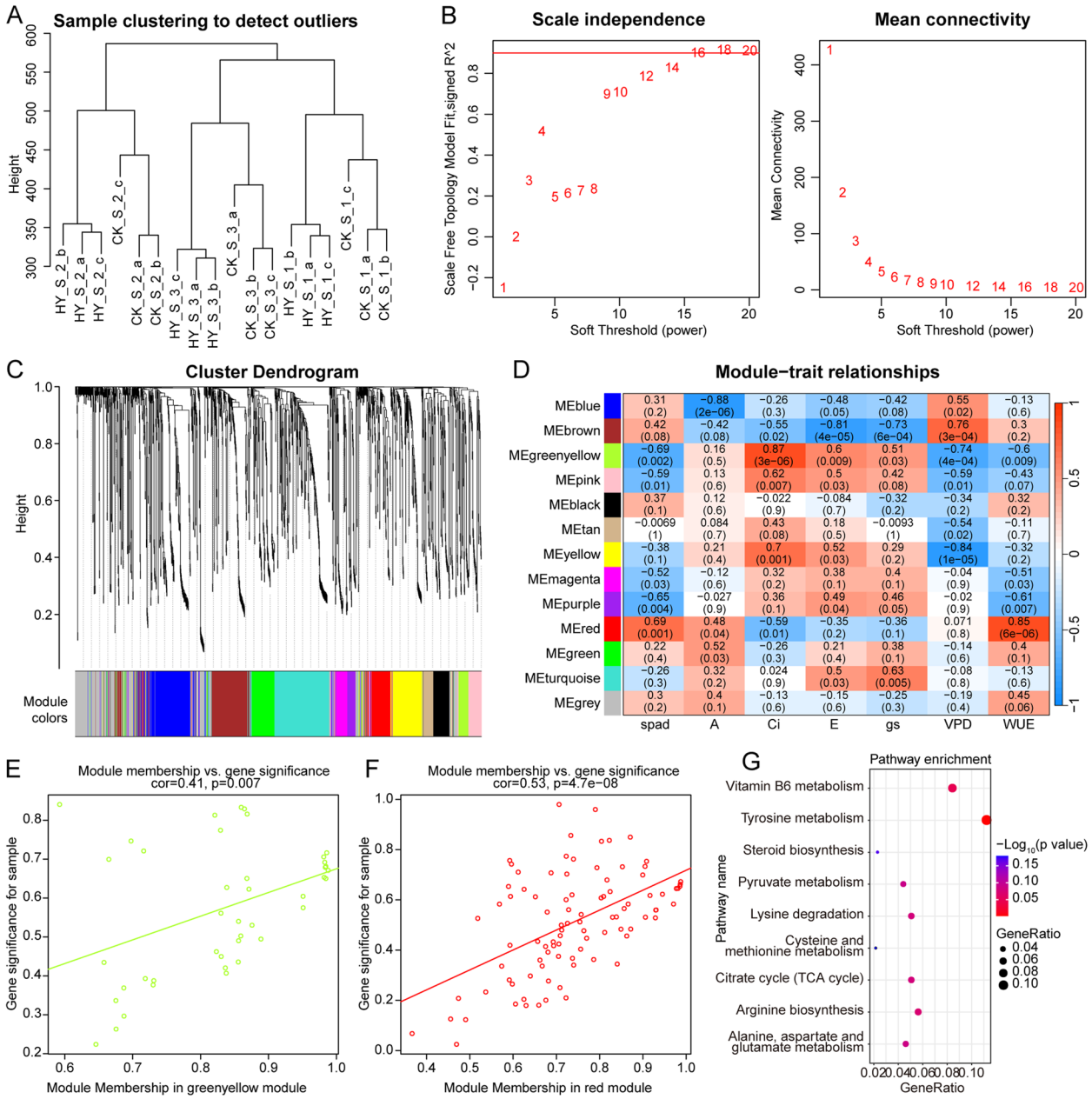

Fig. 5 Identification of SPAD-related metabolites modules by WGCNA. **A** hierarchical clustering tree of the 18 samples. **B** Selection of soft-thresholding power β. **C** Metabolite module and module colors. **D** The correlation between each module and SPAD trait. **E**, **F** Greenyellow and red modules with the highest absolute correlation to SPAD and a *p*-value less than 0.05. **G** KEGG enrichment analysis of metabolites in greenyellow and red modules

Integral analysis of transcriptome and metabolome

DEGs and DEMs were separately correlated with HY group relative to the CK group at three different time points, and Pearson correlation coefficients were computed. Correlations with a p-value < 0.05 were selected for further analysis, and a nine-quadrant diagram (Fig. 7A) was plotted. Common KEGG pathways between DEGs and DEMs were identified at each time point. The results indicated that 32, 26, and 37 shared KEGG pathways in April, May, and June, respectively (Fig. 7B, Table S8). Further intersecting the enrichment results from the three time points revealed both DEGs and DEMs were enriched on 10 KEGG pathways. The pathways included in this analysis were those of biosynthesis of cofactors,

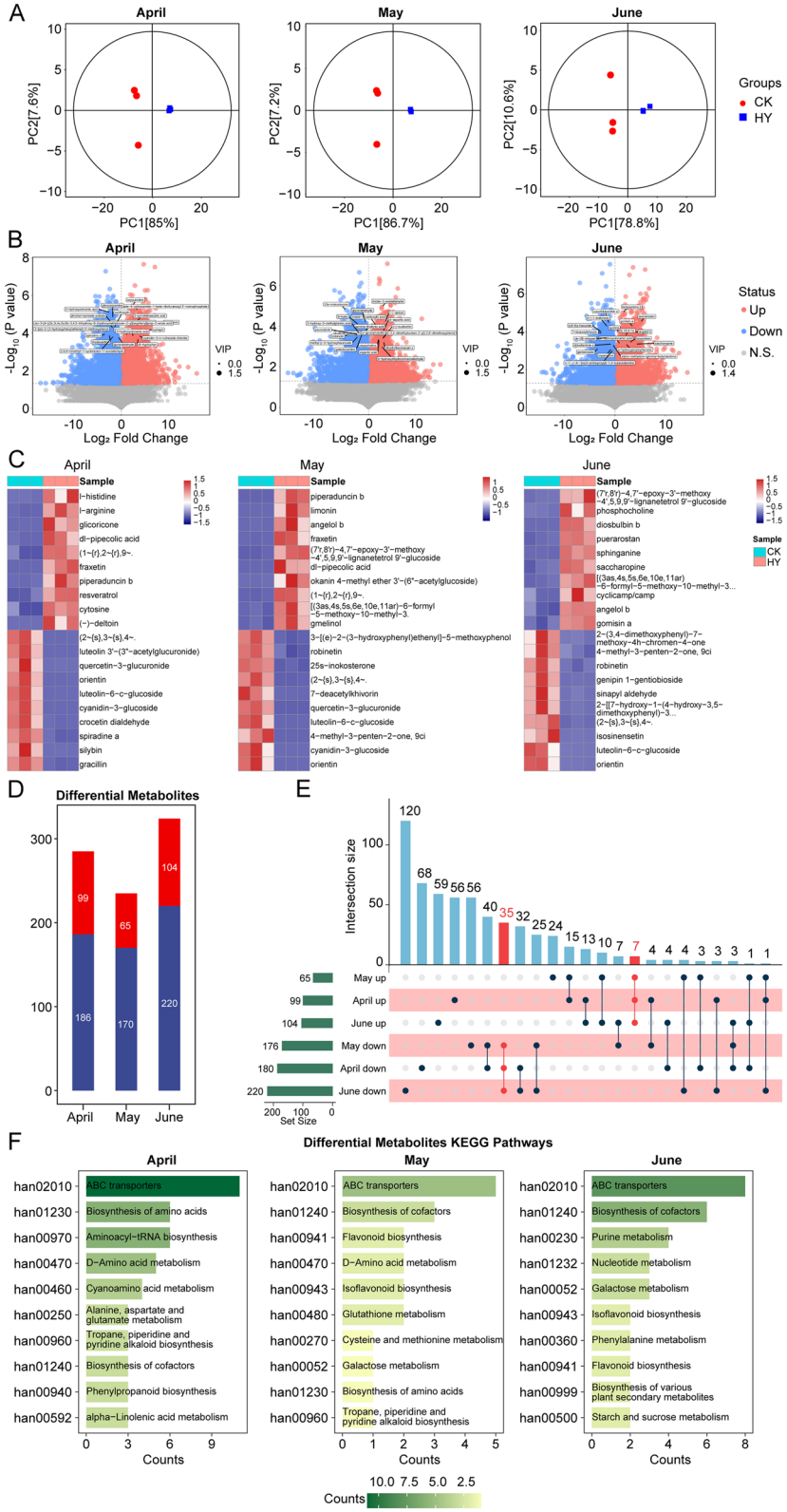

Fig. 6 Differential metabolomics analysis between HY and CK individuals. **A** PCA analysis of metabolites at different time points. **B** Volcano plot of DEMs between HY and CK leaves in April, May, and June. **C** Heatmap of top 10 upregulated and downregulated metabolites in April, May, and June. **D** Quantity of DEMs between HY and CK individuals from April to June. **E** Intersection of DEMs of HY and CK groups at three months. **F** TOP10 enriched KEGG pathways of DEMs between HY and CK leaves at different time points

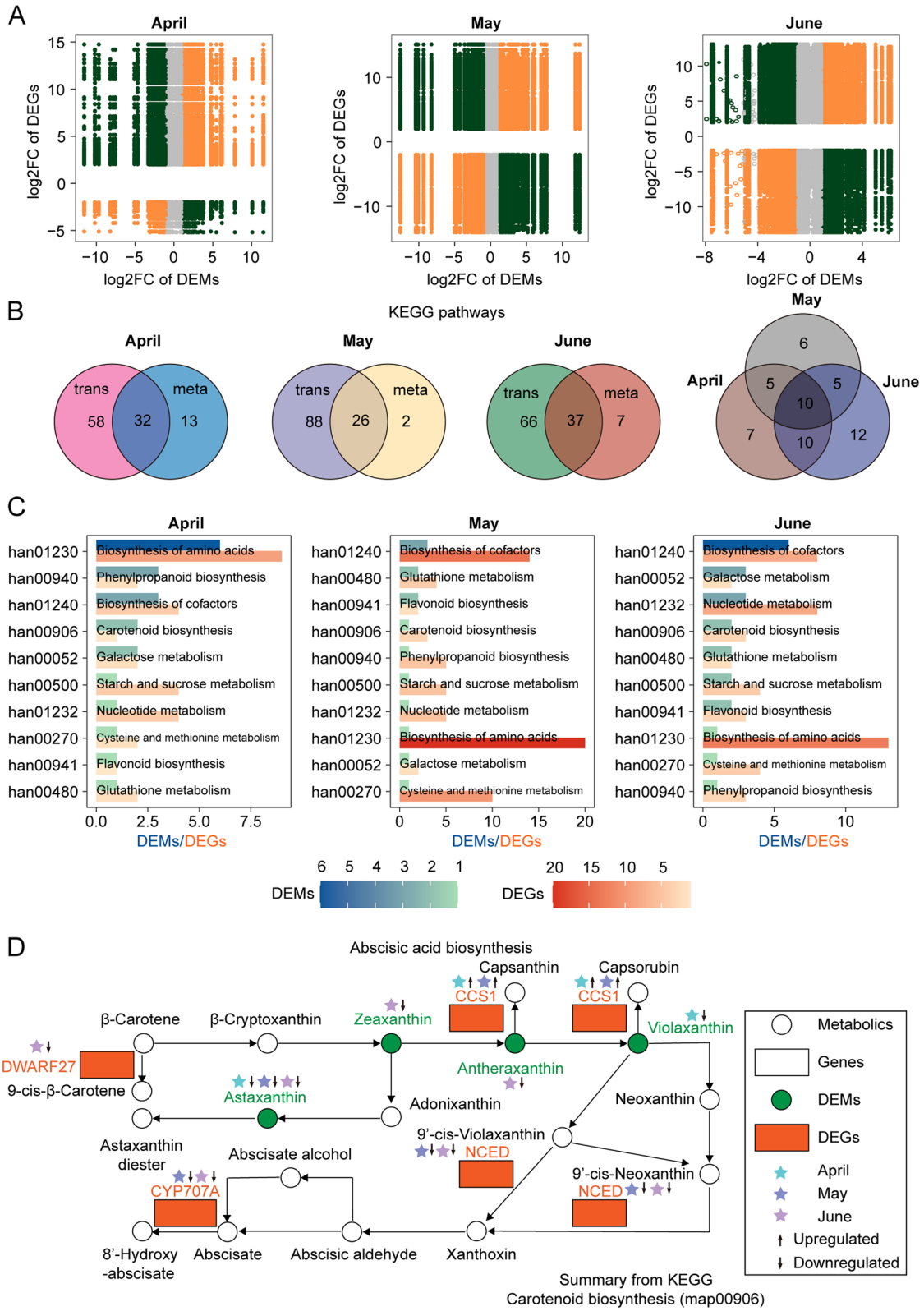

Fig. 7 Integral analysis of transcriptome and metabolome. **A** Nine-quadrant diagram of DEGs and DEMs. **B** KEGG pathways enriched by DEGs and DEMs. **C** Ten KEGG pathways affected by DEGs and DEMs at three time points. **D** ABA biosynthesis-related pathways

nucleotide metabolism, galactose metabolism, flavonoid biosynthesis, starch and sucrose metabolism, glutathione metabolism, carotenoid biosynthesis, phenylpropanoid biosynthesis, cysteine and methionine metabolism, and biosynthesis of amino acids (Fig. 7C).

To gain further insights into the distribution of DEGs and DEMs in the carotenoid biosynthesis signaling pathway, it was observed that they were predominantly concentrated around the abscisic acid (ABA) biosynthesis-related pathways with four types of carotenoid pigments (astaxanthin, zeaxanthin, violaxanthin, antheraxanthin) downregulated (Fig. 7D). In the signaling pathway related to flavonoid synthesis, shikimate O-hydroxycinnamoyltransferase exhibited significant differences between HY and CK leaves from April to June. In June, the significant downregulation of Chalcone synthase might result in significant changes in downstream (-)-Epiafzelechin and Kaempferol metabolic products (Figure. S1). The pathways identified in our study might be crucial for the pigmentation patterns observed in the leaves of *Heliopsis helianthoides*.

Discussion

The leaf color of plants is important for the adaptation to the environment. For variegated-leaf plants, the patches on leaf surfaces play a crucial role in environmental adaptation such as avoidance of predation and reproduction [22]. Additionally, they have garnered attention for their significant value as appealing ornamental plants [23]. Leaf curling is a self-protective mechanism of plants to deal with abiotic stresses such as strong light, drought, salt and heat, further reducing the light-exposed area and the damage to the leaves [24]. In our study, the transcriptome and metabolome of *Heliopsis helianthoides* variegated-leaf HY and green-leaf CK upper leaves from April to June were measured. After confirming the significant morphological and physiological differences (especially chlorophyll content) between the two subtypes, DEGs and DEMs were found to be enriched in carotenoid biosynthesispathway.

Significant differences in SPAD value and chlorophyll contents (total chlorophyll, chlorophyll a and b) between HY and CK suggested the vital influence of chlorophyll in leaf variegation. An interesting finding was that chlorophyll contents of CK samples declined as time passed, while increasing in HY. Despite the significant chlorophyll differences between HY and CK, DEGs hadn't been enriched on chlorophyll-related or chloroplast-related pathways. Long ago, the photosynthetic capacity of higher plants was known to be negatively impacted by iron deficiency, primarily due to the loss of chlorophyll [25, 26]. Particularly, iron deficiency can result in interveinal chlorosis—tissue yellowing between the veins [27, 28], precisely as the HY type in our study. Due to the downregulation of yellow pigments in carotenoid pathway, the "yellowing" tissues show white in HY leaves. The chlorosis becomes obvious in the youngest leaves [29]. In plants, ferritin is a vital protein responsible for the regulation and storage of iron. Plant ferritin plays a key role in ensuring iron homeostasis, facilitating iron transport within plant tissues, supporting photosynthesis, and protecting cells from oxidative stress. In contrast to translational level in animals, ferritins are regulated in transcriptional level in plants [19]. We were able to screen a DEG PFE2 in transcriptome which was annotated as ferritin-4. The downregulation of this gene in all three months was validated by qRT-PCR. The variegation in HY leaves might be partly caused by iron deficiency. In the future, we plan to apply iron fertilizer to the HY subtype to explore whether its variegated leaves will be restored to normal green leaves.

In our study, FSD2 was downregulated in HY compared to CK in all three months. FSD2 is a type of Fe (iron) enzyme superoxide dismutase (SOD) located in the chloroplast of *Arabidopsis* [30]. FSD2 plays an essential role in chloroplast early development. Its mutant has a pale green phenotype, and fsd2 fsd3 double mutant has a severe albino phenotype [20]. In another research, fsd2 mutant has been found to exhibit increased superoxide production, reduced chlorophyll levels, lower PSII efficiency, and a lower rate of CO_2 assimilation [31], which are mostly consistent with HY in our research, where HY displays significantly lower FSD2 expression level compared to CK. HY leaves show interveinal chlorosis, indicating the spatial distribution of chlorophyll. In variegated leaves, the green sectors exhibit morphologically typical chloroplasts, while the lighter parts predominantly contain atypical chloroplasts characterized by reduced chlorophyll and carotenoid pigments [32, 33]. Many genes have been identified to control the variegation in leaves, such as VARIEGATED 2 [34] and IMMUTANS [35], but none of them shows significant expression levels between HY and CK types, probably due to the different variegation types of *Arabidopsis* leaves in those research.

Based on our results concerning the carotenoid signaling pathway, another reason for the absence of significant differential expression in chlorophyll or chloroplast-related genes may be not only chlorophyll influences the leaf color, but other pigments are also downregulated in the HY type, leading to lighter color. In our research, the leaf color indicated by SPAD value was significantly different between HY and CK in June while the chlorophyll content didn't show a significant difference, potentially due to the influence of carotenoid content. Although SPAD mainly reflects the content of chlorophyll, its value

is influenced by other factors such as carotenoids. A linear correlation between SPAD and carotenoids has been identified [36]. In the carotenoid biosynthesis pathway, four types of pigments were found to be downregulated in HY individuals. Astaxanthin is a red fat-soluble carotenoid that acts as an unusual antioxidant [37]. Zeaxanthin is a yellow-orange pigment [38]. Violaxanthin is a natural orange-colored xanthophyll pigment biosynthesized from zeaxanthin [39]. Antheraxanthin is bright yellow. NCED, or 9-cis-epoxycarotenoid dioxygenase, is a key gene in ABA biosynthesis pathway [40]. In peach, downregulation of NCED has been shown to lead carotenoid accumulation because of inhibition of violaxanthin breakdown [41]. What's more, NCED expression may enhance ABA [42]. Long-term exogenous ABA treatment reduces chlorophyll levels [43]. In seeds, ABA is the main regulator of chlorophyll degradation [44]. ABA signaling pathway is also closely related to jasmonate, which is an elicitor for chlorophyll degradation [45]. We deduce that the enhanced chlorophyll degradation might be one of the reasons of HY leaf variegation. Meanwhile, further NCED related details deserve to be investigated in our future study, especially involving its role in HY, which would benefit for the deepening the understanding of leaf color.

It's noteworthy that, ABC transporters were enriched by DEMs between HY and CK samples in April, May and June with the most counts. While ABC transporters themselves do not directly determine leaf color, they may indirectly influence it through their role in various processes in plants. ABC proteins play a pivotal role in regulating a wide array of biological processes in plants, encompassing growth, developmental processes, nutrient acquisition, resilience to both biotic and abiotic stressors, metal toxicity tolerance, and the conveyance of phytohormones, among others [46]. Some ABC transporters are involved in the uptake and transport of essential nutrients, such as amino acids, lipids, sugar, and metals [47], including magnesium. Magnesium is a critical component of chlorophyll [48]. ABC transporters also play a role in the transport of secondary metabolites, including carotenoids [49] discussed above, affecting the coloration of leaves. Furthermore, ABC transporters are responsible for the transport of plant hormones, such as ABA [50], which may induce degradation of chlorophyll. Hence, the dysfunction of ABC transporters may be a contributing factor in the mechanism of variegation in HY leaves.

Conclusions

In our study of exploring the leaf variegation mechanism of HY *Heliopsis helianthoides* subtype, comparison of transcriptome and metabolome with green-leaf CK subtype was performed. Downregulation of FSD2 might be the reason of chlorophyll content reduction in HY. PFE2 (ferritin-4) has been validated to be downregulated in HY subtype, which potentially promotes the variegation phenotype. DEMs between HY and CK were enriched on ABC transporters, indicating potential transporting dysfunction in variegated leaves. The DEGs and DEMs were concentrated on carotenoid biosynthesis pathway, showing a decrease in pigments in HY individuals. This study contributes to the understanding of the leaf variegation mechanism in HY, which may provide insights for future research and potential applications in plant breeding to help maintain the variegated-leaf traits.

Supplementary Information

The online version contains supplementary material available at https://doi.org/10.1186/s12870-024-05450-5.

Supplementary Material 1.
Supplementary Material 2.
Supplementary Material 3.
Supplementary Material 4.
Supplementary Material 5.
Supplementary Material 6.
Supplementary Material 7.
Supplementary Material 8.
Supplementary Material 9.
Supplementary Material 10.

Acknowledgements
Not applicable.

Authors' contributions
Conceptualization: Helan Qin and Jia Guo. Funding acquisition: Yingshan Jin and Zijing Li. Resources: Ju Chen, Zhengwei Bie, and Chunyu Luo. Investigation: Feitong Peng, Dongyan Yan, and Qinggang Kong. Data curation: Fang Liang and Xiuna Cui. Formal analysis: Hua Zhang and Xuefan Hu. Visualization: Rongfeng Cui. Writing-original draft, writing-review and editing: Helan Qin.

Funding
This study was supported by the Beijing Municipal Administration Center Of Parks "Studies on selection, breeding and mass propagation in leaf variegation of New excellent garden plants '*Heliopsis helianthoides*'"[Grant number: ZX2021027], the Beijing Key Laboratory of Greening Plants Breeding "Stuies on key planting techniques for Quercus seedlings in plain forests" [Grant number: YZZD202306 and YZZD202407].

Availability of data and materials
The sequence data for this study are available in the NCBI SRA database (https://www.ncbi.nlm.nih.gov/sra) (Accession:PRJNA1059652).

Declarations

Ethics approval and consent to participate
Not applicable.

Consent for publication
Not applicable.

Competing interests
The authors declare no competing interests.

Author details
[1]Beijing Key Laboratory of Greening Plants Breeding/Beijing Academy of Forestry and Landscape Architecture, No.7 Huajiadi, Chaoyang District, Beijing 100102, China. [2]Beijing Florascape Co., Ltd, No.2 Wenxing Dong Street, Xicheng District, Beijing 100044, China. [3]Beijing Qunfangpu Horticulture Co., Ltd, No.19 Madian East Road, Haidian District, Beijing 100088, China. [4]Beijing Lv Xing Landscaping Co., Ltd, Zhangjiawan Town, Tongzhou District, Beijing 101117, China.

Received: 14 December 2023 Accepted: 23 July 2024
Published online: 31 July 2024

References

1. Zhao M-H, Li X, Zhang X-X, Zhang H, Zhao X-Y. Mutation Mechanism of Leaf Color in Plants: A Review. Forests. 2020;11(8):851.
2. Awan MA, Konzak CF, Rutger JN, Nilan RA. Mutagenic Effects of Sodium Azide in Rice1. Crop Sci. 1980;20(5):cropsci1980.0011183X0020000500 30x. https://doi.org/10.2135/cropsci1980.0011183X002000050030x.
3. Gustafsson A., The plastid development in various types of chlorophyll mutations. Hereditas, 1942: p. 483–492. https://onlinelibrary.wiley.com/doi/pdf/10.1111/j.1601-5223.1942.tb03292.x.
4. Ljubesic N, Wrischer M, Prebeg T, Devidé Z, Boskovic R. Chloroplast structure and function in wild-type and aurea-type leaves of the Japanese spindle-tree over their life span. Acta Bot Croat. 2003;62(1):1–10.
5. Reuter JA, Spacek DV, Snyder MP. High-throughput sequencing technologies. Mol Cell. 2015;58(4):586–97. https://doi.org/10.1016/j.molcel.2015.05.004.
6. Zhang S, Wu X, Cui J, Zhang F, Wan X, Liu Q, et al. Physiological and transcriptomic analysis of yellow leaf coloration in Populus deltoides Marsh. PLoS ONE. 2019;14(5):e0216879. https://doi.org/10.1371/journal.pone.0216879.
7. Zhu L, Wen J, Ma Q, Yan K, Du Y, Chen Z, et al. Transcriptome profiling provides insights into leaf color changes in two Acer palmatum genotypes. BMC Plant Biol. 2022;22(1):589. https://doi.org/10.1186/s12870-022-03979-x.
8. Agati G, Azzarello E, Pollastri S, Tattini M. Flavonoids as antioxidants in plants: location and functional significance. Plant Sci. 2012;196:67–76. https://doi.org/10.1016/j.plantsci.2012.07.014.
9. Chen M, Chang C, Li H, Huang L, Zhou Z, Zhu J, et al. Metabolome analysis reveals flavonoid changes during the leaf color transition in Populus x euramericana "Zhonghuahongye." Front Plant Sci. 2023;14:1162893. https://doi.org/10.3389/fpls.2023.1162893.
10. Wang Y, Zhen J, Che X, Zhang K, Zhang G, Yang H, et al. Transcriptomic and metabolomic analysis of autumn leaf color change in Fraxinus angustifolia. PeerJ. 2023;11:e15319. https://doi.org/10.7717/peerj.15319.
11. Chen S, Zhou Y, Chen Y, Gu J. fastp: an ultra-fast all-in-one FASTQ preprocessor. Bioinformatics. 2018;34(17):i884–90. https://doi.org/10.1093/bioinformatics/bty560.
12. Grabherr MG, Haas BJ, Yassour M, Levin JZ, Thompson DA, Amit I, et al. Full-length transcriptome assembly from RNA-Seq data without a reference genome. Nat Biotechnol. 2011;29(7):644–52. https://doi.org/10.1038/nbt.1883.
13. Langfelder P, Horvath S. WGCNA: an R package for weighted correlation network analysis. BMC Bioinformatics. 2008;9:559. https://doi.org/10.1186/1471-2105-9-559.
14. Zhang B and Horvath S. A General Framework for Weighted Gene Co-Expression Network Analysis. Stat Appl Genet Mol Biol. 2005;4(1). https://doi.org/10.2202/1544-6115.1128.
15. Love MI, Huber W, Anders S. Moderated estimation of fold change and dispersion for RNA-seq data with DESeq2. Genome Biol. 2014;15(12):550. https://doi.org/10.1186/s13059-014-0550-8.
16. Yu G, Wang LG, Han Y, He QY. clusterProfiler: an R package for comparing biological themes among gene clusters. OMICS. 2012;16(5):284–7. https://doi.org/10.1089/omi.2011.0118.
17. Livak KJ, Schmittgen TD. Analysis of relative gene expression data using real-time quantitative PCR and the 2(-Delta Delta C(T)) Method. Methods. 2001;25(4):402–8. https://doi.org/10.1006/meth.2001.1262.
18. Smith CA, Want EJ, O'Maille G, Abagyan R, Siuzdak G. XCMS: processing mass spectrometry data for metabolite profiling using nonlinear peak alignment, matching, and identification. Anal Chem. 2006;78(3):779–87. https://doi.org/10.1021/ac051437y.
19. Briat JF, Ravet K, Arnaud N, Duc C, Boucherez J, Touraine B, et al. New insights into ferritin synthesis and function highlight a link between iron homeostasis and oxidative stress in plants. Ann Bot. 2010;105(5):811–22. https://doi.org/10.1093/aob/mcp128.
20. Myouga F, Hosoda C, Umezawa T, Iizumi H, Kuromori T, Motohashi R, et al. A heterocomplex of iron superoxide dismutases defends chloroplast nucleoids against oxidative stress and is essential for chloroplast development in Arabidopsis. Plant Cell. 2008;20(11):3148–62. https://doi.org/10.1105/tpc.108.061341.
21. Iwashina T. Contribution to flower colors of flavonoids including anthocyanins: a review. Nat Prod Commun. 2015;10(3):529–44.
22. Shelef O, Summerfield L, Lev-Yadun S, Villamarin-Cortez S, Sadeh R, Herrmann I, et al. Thermal Benefits From White Variegation of Silybum marianum Leaves. Front Plant Sci. 2019;10:688. https://doi.org/10.3389/fpls.2019.00688.
23. Zhang J-H, Zeng J-C, Wang X-M, Chen S-F, Albach DC, Li H-Q. A revised classification of leaf variegation types. Flora. 2020;272:151703. https://doi.org/10.1016/j.flora.2020.151703.
24. Merrium S, Ali Z, Tahir MHN, Habib-Ur-Rahman M, Hakeem S. Leaf rolling dynamics for atmospheric moisture harvesting in wheat plant as an adaptation to arid environments. Environ Sci Pollut Res Int. 2022;29(32):48995–9006. https://doi.org/10.1007/s11356-022-18936-2.
25 Marsh HV, Evans HJ, Matrone G. Investigations of the Role of Iron in Chlorophyll Metabolism. II. Effect of iron deficiency on chlorophyll synthesis. Plant Physiol. 1963;38(6):638–42. https://doi.org/10.1104/pp.38.6.638.
26. Pushnik JC, Miller GW, Manwaring JH. The role of iron in higher plant chlorophyll biosynthesis, maintenance and chloroplast biogenesis. J Plant Nutr. 1984;7(1–5):733–58. https://doi.org/10.1080/01904168409363238.
27. El Amine B, Mosseddaq F, Naciri R, Oukarroum A. Interactive effect of Fe and Mn deficiencies on physiological, biochemical, nutritional and growth status of soybean. Plant Physiol Biochem. 2023;199:107718. https://doi.org/10.1016/j.plaphy.2023.107718.
28. Kaya C, Ashraf M. The mechanism of hydrogen sulfide mitigation of iron deficiency-induced chlorosis in strawberry (Fragaria x ananassa) plants. Protoplasma. 2019;256(2):371–82. https://doi.org/10.1007/s00709-018-1298-x.
29. Lerner, R. Interveinal Chlorosis on Azaleas and Rhododendron. 2011 Feb. 22]; Available from: https://www.purdue.edu/hla/sites/yardandgarden/interveinal-chlorosis-on-azaleas-and-rhododendron/.
30. Kliebenstein DJ, Monde RA, Last RL. Superoxide dismutase in Arabidopsis: an eclectic enzyme family with disparate regulation and protein localization. Plant Physiol. 1998;118(2):637–50. https://doi.org/10.1104/pp.118.2.637.
31. Gallie DR, Chen Z. Chloroplast-localized iron superoxide dismutases FSD2 and FSD3 are functionally distinct in Arabidopsis. PLoS ONE. 2019;14(7):e0220078. https://doi.org/10.1371/journal.pone.0220078.
32. Rodermel S. Pathways of plastid-to-nucleus signaling. Trends Plant Sci. 2001;6(10):471–8. https://doi.org/10.1016/s1360-1385(01)02085-4.
33. Ren J, Zou J, Zou X, Song G, Gong Z, Liu Z, et al., Fine Mapping of BoVl Conferring the Variegated Leaf in Ornamental Kale (Brassica oleracea var. acephala). Int J Mol Sci, 2022;23(23). https://doi.org/10.3390/ijms232314853.
34. Chen M, Choi Y, Voytas DF, Rodermel S. Mutations in the Arabidopsis VAR2 locus cause leaf variegation due to the loss of a chloroplast FtsH protease. Plant J. 2000;22(4):303–13. https://doi.org/10.1046/j.1365-313x.2000.00738.x.
35. Carol P, Stevenson D, Bisanz C, Breitenbach J, Sandmann G, Mache R, et al. Mutations in the Arabidopsis gene IMMUTANS cause a variegated phenotype by inactivating a chloroplast terminal oxidase associated with phytoene desaturation. Plant Cell. 1999;11(1):57–68. https://doi.org/10.1105/tpc.11.1.57.
36 Kumar P, Sharma RK. Development of SPAD value-based linear models for non-destructive estimation of photosynthetic pigments in wheat

(Triticum aestivum L.). Indian J Genet Plant Breed. 2019;79(1):96–9. https://doi.org/10.31742/IJGPB.79.1.13.
37. Higuera-Ciapara I, Felix-Valenzuela L, Goycoolea FM. Astaxanthin: a review of its chemistry and applications. Crit Rev Food Sci Nutr. 2006;46(2):185–96. https://doi.org/10.1080/10408690590957188.
38. el Abdel-Aal SM, Akhtar H, Zaheer K, Ali R. Dietary sources of lutein and zeaxanthin carotenoids and their role in eye health. Nutrients. 2013;5(4):1169–85. https://doi.org/10.3390/nu5041169.
39. Meléndez-Martínez AJ, Britton G, Vicario IM, Heredia FJ. The complex carotenoid pattern of orange juices from concentrate. Food Chem. 2008;109(3):546–53. https://doi.org/10.1016/j.foodchem.2008.01.003.
40. Gan Z, Shan N, Fei L, Wan C, Chen J. Isolation of the 9-cis-epoxycarotenoid dioxygenase (NCED) gene from kiwifruit and its effects on postharvest softening and ripening. Sci Hortic. 2020;261:109020. https://doi.org/10.1016/j.scienta.2019.109020.
41. Song H, Liu J, Chen C, Zhang Y, Tang W, Yang W, et al. Down-regulation of NCED leads to the accumulation of carotenoids in the flesh of F(1) generation of peach hybrid. Front Plant Sci. 2022;13:1055779. https://doi.org/10.3389/fpls.2022.1055779.
42. Gavassi MA, Silva GS, da Silva CDMS, Thompson AJ, Macleod K, Oliveira PMR, et al. NCED expression is related to increased ABA biosynthesis and stomatal closure under aluminum stress. Environ Exp Bot. 2021;185:104404. https://doi.org/10.1016/j.envexpbot.2021.104404.
43. Wang M, Lee J, Choi B, Park Y, Sim HJ, Kim H, et al. Physiological and Molecular Processes Associated with Long Duration of ABA Treatment. Front Plant Sci. 2018;9:176. https://doi.org/10.3389/fpls.2018.00176.
44. Smolikova G, Dolgikh E, Vikhnina M, Frolov A and Medvedev S. Genetic and Hormonal Regulation of Chlorophyll Degradation during Maturation of Seeds with Green Embryos. Int J Mol Sci. 2017;18(9). https://doi.org/10.3390/ijms18091993.
45. Yu Q, Hua X, Yao H, Zhang Q, He J, Peng L, et al. Abscisic acid receptors are involves in the Jasmonate signaling in Arabidopsis. Plant Signal Behav. 2021;16(10):1948243. https://doi.org/10.1080/15592324.2021.1948243.
46. Dahuja A, Kumar RR, Sakhare A, Watts A, Singh B, Goswami S, et al. Role of ATP-binding cassette transporters in maintaining plant homeostasis under abiotic and biotic stresses. Physiol Plant. 2021;171(4):785–801. https://doi.org/10.1111/ppl.13302.
47. Rees DC, Johnson E, Lewinson O. ABC transporters: the power to change. Nat Rev Mol Cell Biol. 2009;10(3):218–27. https://doi.org/10.1038/nrm2646.
48. Ishfaq M, Wang Y, Yan M, Wang Z, Wu L, Li C, et al. Physiological Essence of Magnesium in Plants and Its Widespread Deficiency in the Farming System of China. Front Plant Sci. 2022;13:802274. https://doi.org/10.3389/fpls.2022.802274.
49. Yazaki K. ABC transporters involved in the transport of plant secondary metabolites. FEBS Lett. 2006;580(4):1183–91. https://doi.org/10.1016/j.febslet.2005.12.009.
50. Kuromori T, Miyaji T, Yabuuchi H, Shimizu H, Sugimoto E, Kamiya A, et al. ABC transporter AtABCG25 is involved in abscisic acid transport and responses. Proc Natl Acad Sci U S A. 2010;107(5):2361–6. https://doi.org/10.1073/pnas.0912516107.

Publisher's Note